The Journal of Chemical Physics

RESEARCH ARTICLE | MAY 06 2024

Dissipative particle dynamics for coarse-grained models

Special Collection: 2024 JCP Emerging Investigators Special Collection

Tine Curk

J. Chem. Phys. 160, 174115 (2024)
https://doi.org/10.1063/5.0197112

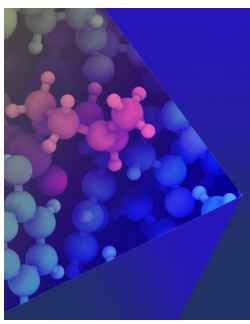

The Journal of Chemical Physics ARTICLE pubs.aip.org/aip/jcp

Dissipative particle dynamics for coarse-grained models

Cite as: J. Chem. Phys. 160, 174115 (2024); doi: 10.1063/5.0197112
Submitted: 11 January 2024 • Accepted: 14 April 2024 •
Published Online: 6 May 2024

Tine Curk[a)]

AFFILIATIONS

Department of Materials Science and Engineering, Johns Hopkins University, Baltimore, Maryland 21218, USA

Note: This paper is part of the 2024 JCP Emerging Investigators Special Collection.
[a)]**Author to whom correspondence should be addressed:** tcurk@jhu.edu

ABSTRACT

We develop a computational method based on Dissipative Particle Dynamics (DPD) that introduces solvent hydrodynamic interactions to coarse-grained models of solutes, such as ions, molecules, or polymers. DPD-solvent (DPDS) is a fully off-lattice method that allows straightforward incorporation of hydrodynamics at desired solvent viscosity, compressibility, and solute diffusivity with any particle-based solute model. Solutes interact with the solvent only through the DPD thermostat, which ensures that the equilibrium properties of the solute system are not affected by the introduction of the DPD solvent, while the thermostat coupling strength sets the desired solute diffusivity. Thus, DPDS can be used as a replacement for traditional molecular dynamics thermostats such as Nosé–Hoover and Langevin. We demonstrate the applicability of DPDS in the case of polymer dynamics and electroosmotic flow through a nanopore. The method should be broadly useful as a means to introduce hydrodynamic interactions to existing coarse-grained models of solutes and soft materials.

I. INTRODUCTION

Coarse-grained implicit-solvent models are usually parameterized to produce a desired equilibrium distribution of states. Using the same models in non-equilibrium simulations with desired transport properties and hydrodynamic behavior requires a method that introduces hydrodynamic interactions at the specific solvent viscosity, compressibility, and solute diffusivity without affecting the equilibrium configurational properties of the system.

To achieve this, the coarse-grained system can be coupled to a mesh, typically a cubic grid, and hydrodynamics is solved using this mesh. A few examples of such approaches include Multi-Particle Collision (MPC) dynamics or Stochastic Rotation Dynamics (SRD),[1,2] Lattice Boltzmann (LB) methods,[3] and Fluid Particle Dynamics (FPD).[4] However, coupling the continuous system to a mesh can introduce artifacts and increase propagation errors. MPC does not conserve angular momentum (or breaks time-reversal symmetry) and suffers from artificially high compressibility.[2] LB allows the embedding of large colloids, but the embedding of particles smaller than the lattice size, e.g., polymers, suffers from lattice discretization errors, and mixing molecular dynamics with LB propagation leads to energy conservation issues.[5] FPD directly solves the Navier–Stokes equations but can only embed objects in at least a few lattice sites in size, which makes the method suitable for nanoparticles and colloids[6] but computationally inefficient for small molecules, ions, or polymers.

Among off-lattice approaches, the most straightforward way to partially introduce hydrodynamics is to apply a Galilean-invariant thermostat directly to the solute particles;[7] however, this approach requires a dense suspension and is not applicable to dilute solutions. A general off-lattice method is Dissipative Particle Dynamics (DPD), which simulates hydrodynamic interactions by representing the fluid as soft particles.[8,9] DPD reproduces the desired solvent viscosity and compressibility while describing thermal fluctuations and allowing the explicit representation of different chemical components.[10] However, simply adding DPD particles to a coarse-grained system introduces solvation and depletion effects and, thus, changes the equilibrium properties of the system. To overcome these problems, the solute model must be designed for a specific DPD solvent parameterization, and typically the solute–solute interaction is restricted to the soft DPD repulsive interaction, which significantly limits the space of solute models. For example, point charges cannot be included due to electrostatic divergence issues when combined with the DPD soft repulsive potentials.[11] While it is possible to model a variety of multicomponent systems by modifying the conservative interactions between DPD particles,[12–14] this approach

requires careful parameterization; altering conservative interactions does not merely change the equilibrium properties but also transport behavior such as local viscosity, compressibility, and diffusivity.

Here, we propose an alternative off-lattice method, named DPD solvent (DPDS), that incorporates hydrodynamic interactions in coarse-grained models of solutes. The premise of the method is to overlay the DPD fluid at the desired viscosity and compressibility with the solute system. The DPD solvent interacts with the solute system only via the DPD thermostat. Thus, the equilibrium properties of the system and the DPD-solvent are fully decoupled and can be controlled separately, while the transport properties are determined by the solute–solvent thermostat coupling strength. The main advantage of this procedure over existing lattice methods is that it avoids any lattice mapping issues. The same or a similar velocity-Verlet integrator is used to evolve configurations both for the solute system and the DPD solvent, which minimizes propagation errors due to solvent–solute coupling and significantly simplifies the implementation compared to hybrid lattice approaches. The main advantage of DPDS over standard DPD is that DPDS can be directly used with any solute model and is not restricted to soft DPD repulsive potentials. This enables straightforward simulations of charged particles and the introduction of hydrodynamic interactions to already developed solute models. Moreover, hydrodynamic interactions can be switched on/off without affecting any equilibrium properties of the solute system, allowing direct evaluation of hydrodynamic effects compared to, for example, Langevin dynamics.

In the following, we review the DPD technique and then show how to combine it with coarse-grained systems of solutes using the DPDS approach. We demonstrate the applicability of DPDS on two typical coarse-grained models, a bead–spring polymer and an electrolyte solution, and show that it accurately describes hydrodynamic interactions by investigating polymer collapse, Zimm dynamics, and electrokinetic flow in patterned nanochannels.

II. REVIEW OF THE DPD FLUID PROPERTIES

The DPD fluid is modeled as a canonical ensemble of soft, spherical particles at density ρ and temperature T. The particles interact via three distinct interactions. The conservative pair interaction is typically chosen as parabolic repulsion, with the potential energy of an ensemble of N particles,

$$V(\mathbf{r}^N) = \frac{1}{2}\sum_{ij}\begin{cases} a_{ij}(1 - r_{ij}/r_c)^2 & \text{for } r_{ij} < r_c, \\ 0, & \text{otherwise.} \end{cases} \tag{1}$$

The sum proceeds over all particle pairs i, j, with $\mathbf{r}_i$ the position of particle i, $r_{ij} = |\mathbf{r}_i - \mathbf{r}_j|$ the inter-particle distance, and r_c the cutoff length. The prefactor a_{ij} is set to reproduce the desired compressibility of the fluid[9] and can be different among different particle types to model multicomponent fluids.

The dissipative friction force between particles i and j is

$$F_{ij}^{\mathrm{d}} = \gamma\omega(r_{ij})^2(\mathbf{v}_{ij}\cdot\hat{\mathbf{r}}_{ij})\hat{\mathbf{r}}_{ij} - \gamma_\perp\omega_\perp(r_{ij})^2(\mathbf{I} - \hat{\mathbf{r}}_{ij}\hat{\mathbf{r}}_{ij}^T)\mathbf{v}_{ij}, \tag{2}$$

where the first term describes the friction force parallel to the inter-particle vector $\mathbf{r}_{ij} = \mathbf{r}_j - \mathbf{r}_i$ with $\hat{\mathbf{r}}_{ij} = \mathbf{r}_{ij}/|\mathbf{r}_{ij}|$ the corresponding unit vector. The friction is proportional to the coefficient γ and the distance-dependent weighting function $\omega(r_{ij})$. The second term describes the corresponding perpendicular contribution,[15] i.e., the shear friction, with coefficient $\gamma_\perp$ and weighting function $w_\perp(r_{ij})$. $\mathbf{I}$ is the identity matrix, and $\hat{\mathbf{r}}_{ij}^T$ denotes the transpose of $\hat{\mathbf{r}}_{ij}$.

The fluctuation–dissipation relation implies that the random force between the two particles is given by

$$F_{ij}^{\mathrm{r}} = \sqrt{2\gamma k_{\mathrm{B}}T}\,\omega(r_{ij})\frac{dW_{ij}}{dt}\hat{\mathbf{r}}_{ij} + \sqrt{2\gamma_\perp k_{\mathrm{B}}T}\,\omega_\perp(r_{ij})\frac{d\mathbf{W}_{ij}}{dt}(\mathbf{I} - \hat{\mathbf{r}}_{ij}\hat{\mathbf{r}}_{ij}^T), \tag{3}$$

where the prefactors are determined by the desired temperature T of the system, dW_{ij} is the independent increment of a Wiener process, and $d\mathbf{W}_{ij}$ is the vector of independent Wiener processes. For a finite time-step $\sim\Delta t$, $\frac{\Delta W_{ij}}{\Delta t} = \zeta_{ij}\Delta t^{-1/2}$ and $\frac{\Delta \mathbf{W}_{ij}}{\Delta t} = \boldsymbol{\zeta}_{ij}\Delta t^{-1/2}$, where ζ_{ij} is a symmetric random variable with zero mean and unit variance and $\boldsymbol{\zeta}_{ij}$ is the corresponding random vector.

The stochastic differential equations that determine the evolution of the fluid are,

$$m_i\frac{d\mathbf{v}_i}{dt} = -\frac{\partial V}{\partial \mathbf{r}_i} + \sum_j F_{ij}^{\mathrm{d}} + F_{ij}^{\mathrm{r}}, \qquad \frac{d\mathbf{r}_i}{dt} = \mathbf{v}_i, \tag{4}$$

with m the mass of the DPD particles. These equations are usually evolved using the velocity-Verlet integrator,[9,16] and the DPD model is implemented in various open-source molecular dynamics (MD) packages such as the Large-scale Atomic/Molecular Massively Parallel Simulator (LAMMPS), EPResSo, and HOOMD-blue. Since the dissipative and random forces act only on relative velocities, the integrator preserves Galilean invariance and conserves momentum, implying that the behavior of the fluid follows Navier–Stokes hydrodynamics on sufficiently large length scales.

When applied to molecular simulations, the main advantage of DPD compared to Langevin dynamics or finite element hydrodynamic solvers is that the DPD method simultaneously samples the correct canonical (N, V, T) Gibbs–Boltzmann ensemble, preserves hydrodynamics, and can capture chemical specificity. Consequently, the method has been widely used to simulate hydrodynamic interactions in various systems, including colloidal suspensions, blood, phase-separating fluids, polymer solutions, electrolytes, and biological membranes; see Refs. 10 and 17 for extensive reviews of DPD fundamentals and applications.

In the following, we use standard parameters corresponding to an aqueous solution with each DPD particle representing $N_{\mathrm{w}} = 3$ water molecules: the particle density $\rho_{\mathrm{s}} = 3/r_c^3$, with the cutoff $r_c = 0.646$ nm, which is taken as the length unit $\lambda = r_c$, and the interaction prefactor $a_{ij} = 78k_{\mathrm{B}}T$ reproduces the compressibility of water at room temperature.[9] To reduce the number of parameters, the dissipative weighing function $w(r_{ij})$ has the same form as the conservative repulsive force, a common choice for DPD simulations,[10]

$$w(r_{ij}) = 1 - \frac{r_{ij}}{r_c}. \tag{5}$$

The friction coefficient γ determines the crossover timescale between the ballistic and diffusive regimes, $\tau_{\mathrm{BD}} \sim m/\gamma$ (an exact calculation is provided below). The typical choice for the friction parameter is $\gamma = 4.5\sqrt{k_{\mathrm{B}}Tm}/r_{\mathrm{c}}$,[9] which ensures that the dynamics is diffusive on all relevant length scales ($r \geq r_{\mathrm{c}}$) and time scales ($t \geq \tau$), where the molecular dynamics time unit τ, which measures the characteristic time required to move ballistically by a distance r_{c}, is $\tau = r_{\mathrm{c}}\sqrt{m/(k_{\mathrm{B}}T)}$. The original DPD formulation used no shear friction ($\gamma_{\perp} = 0$),[9] but its inclusion has been shown to improve hydrodynamic properties,[15] so we use $\gamma_{\perp} = \gamma$ and $w_{\perp}(r_{ij}) = w(r_{ij})$.[18]

We note that employing these standard DPD parameters contains the inherent limitation that the Schmidt number $\mathrm{Sc} = \nu_{\mathrm{k}}/D$, which measures the ratio of momentum diffusion to mass diffusion, with ν_{k} the kinematic viscosity and D the diffusion constant, is too low. $\mathrm{Sc} \sim 7$ for the DPD fluid, which is much smaller than $\mathrm{Sc} \sim 370$ expected for water at room temperature ($T = 298$ K) and standard pressure.[9,18] This discrepancy is a consequence of using a soft repulsive potential [Eq. (1)] and relatively weak friction that together allow for significantly larger time-steps, which increases the efficiency of the method by about four orders of magnitude compared to atomistic simulations.[13] However, the low Schmidt number does not appear to affect the transport properties of polymers as long as momentum diffusion is faster than mass diffusion ($\mathrm{Sc} > 1$).[19] Moreover, for the majority of nanoscale systems, hydrodynamic flows occur in the low Reynolds number regime ($\mathrm{Re} < 1$), in which case inertia is irrelevant and, thus, an incorrect Schmidt number is not expected to affect any observables. If required, high Schmidt numbers can be obtained by increasing the friction coefficient γ, modifying the weighing function $w(r_{ij})$, at a cost of efficiency,[18,20] or by using the Lowe thermostat.[21] We stress that the proposed DPDS method is general and can be applied to any DPD parameters that model higher Schmidt numbers or non-aqueous solutions.

The simulation time scale τ is determined by setting the desired dynamic viscosity η of the fluid. The viscosity of the DPD fluid can be measured via self-diffusivity, the decay of the stress autocorrelation function, or the Poiseuille profile.[18,22] At the standard parameters used, the viscosity obtained by fitting the Poiseuille profile is $\eta = (2.31 \pm 0.05)k_{\mathrm{B}}T\tau r_{\mathrm{c}}^{-3}$ (see Sec. IV B), which is consistent with the value obtained by the decay of the stress autocorrelation function ($\nu_{\mathrm{k}} = 0.748k_{\mathrm{B}}T\tau m^{-1}$, at $\rho = 3r_{\mathrm{c}}^{-3}$).[18] To model the dynamic viscosity of water, $\eta = 10^{-3}$ Pa s, at room temperature, $T = 298$ K, the MD simulation time scale is thus $\tau = 29$ ps.[23]

III. DPD SOLVENT

We aim to incorporate hydrodynamic interactions within an existing system of solutes, such as ions, molecules, polymers, or nanoparticles. The premise of the DPDS method that achieves this is:

(i) There are no conservative interactions between the system and the DPD fluid. This requirement ensures that all equilibrium configurational observables of the system are not affected by the presence of the DPD solvent. The DPD solvent parameters (a_{ij}, γ) are set to reproduce the desired compressibility and viscosity of the solvent.

(ii) The system interacts with the solvent via the DPD thermostat, whose coupling is set to reproduce the desired diffusion constant of the solutes. In particular, a system containing N_{s} solute particles is described by interactions that define the potential energy $V_{\mathrm{s}}(\mathbf{r}_{\mathrm{s}}^{N_{\mathrm{s}}})$ depending on the positions $\mathbf{r}_{\mathrm{s}}^{N_{\mathrm{s}}}$ of these solute particles. To preserve the equilibrium distribution of configurational states, the DPD fluid is coupled to the solutes only via random and dissipative forces [Eqs. (2) and (3)], and the solute–DPD coupling is determined by the strength γ_{s} and the weighting function $w_{\mathrm{s}}(r_{ij})$. To simplify the implementation and reduce the number of parameters, $w_{\mathrm{s}}(r_{ij})$ has the same form as between DPD particles, Eq. (5), but with a different cutoff value, r_{s},

$$w_{\mathrm{s}}(r_{ij}) = 1 - \frac{r_{ij}}{r_{\mathrm{s}}}, \tag{6}$$

where the index i refers to solutes and the index j to solvent (DPD) particles. We stress that there is nothing special about this form; Eq. (6) is chosen for convenience, but any other peaked function could be used. There are no direct, dissipative, or random forces between solvent particles. The perpendicular and parallel coupling strengths and weighing functions are chosen to be the same: $\gamma_{\perp,\mathrm{s}} = \gamma_{\mathrm{s}}$ and $w_{\perp,\mathrm{s}}(r_{ij}) = w_{\mathrm{s}}(r_{ij})$. Thus, the solute–solvent coupling is determined by just two parameters: strength γ_{s} and range r_{s}. The range r_{s} is determined by the size of the solute, including the solvation layer, and γ_{s} by the desired solute diffusion constant D.

The solute–solvent hydrodynamic coupling [Eq. (6)] is spherically symmetric, which is applicable to the large majority of coarse-grained models that are based on spherically symmetric excluded-volume interactions, such as monomers in a bead–spring polymer,[24] ions, force-fields such as MARTINI,[25] or DNA/RNA models such as oxDNA.[26] Non-spherically symmetric cases are discussed later.

The diffusion constant $D = D(r_{\mathrm{s}}, \gamma_{\mathrm{s}})$ measured via the mean-squared displacement is shown in Fig. 1. The diffusion constant scaling can also be estimated analytically. Strong coupling, $\gamma_{\mathrm{s}} \to \infty$, implies the solvent is rigidly coupled to the solute within range r_{s}, thus the solute behaves as a solid sphere with radius r_{s} whose diffusivity is given by the Stokes–Einstein relation, $D = k_{\mathrm{B}}T/(6\pi\eta r_{\mathrm{s}})$. Conversely, in the weak coupling regime, the diffusion constant can be calculated by mapping the thermostat forces to a Langevin equation,[9] which yields the diffusion constant $D = 15k_{\mathrm{B}}T/2\pi\gamma_{\mathrm{s}}\rho r_{\mathrm{s}}^3$ (note that this expression is a factor 3 smaller than the result in Ref. 9 due to the inclusion of shear forces, $\gamma_{\perp,\mathrm{s}} = \gamma_{\mathrm{s}}$). These two limits imply the following functional form for the diffusion constant of the solutes:

$$D(r_{\mathrm{s}}, \gamma_{\mathrm{s}}) = \frac{k_{\mathrm{B}}T}{2\pi r_{\mathrm{s}}}\left(\frac{1}{3\eta} + \frac{15}{\rho\gamma_{\mathrm{s}}r_{\mathrm{s}}^2}\right). \tag{7}$$

Using this scaling, the simulation data collapses to a master plot and follows Eq. (7) to within ≈30% (Fig. 2). Therefore, Eq. (7) can be used to estimate γ_{s} given a desired diffusion constant D and solute size r_{s}. If the thermostat without shear forces is used ($\gamma_{\perp,\mathrm{s}} = 0$), the second term in Eq. (7) should be multiplied by a factor of 3.

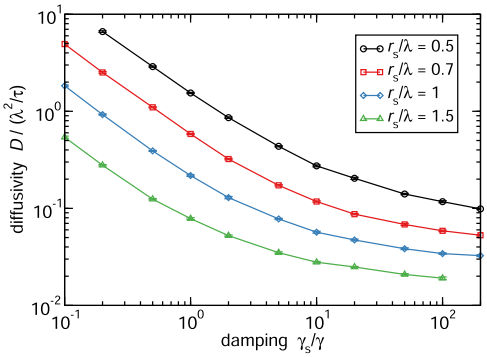

FIG. 1. Diffusion constant depending on the solute size r_s and coupling strength γ_s. Data obtained by simulating system size $L = 100\lambda$ at dilute solute density $\rho_s = 10^{-3}\lambda^{-3}$ and timestep $\Delta t = 10^{-3}\tau$ at the standard DPD parameters: $r_c = \lambda$, $\rho = 3r_c^{-3}$, $a_{ij} = 78k_BT$, and $\gamma = 4.5k_BT\tau r_c^{-2}$. $D = \langle r^2\rangle/(6\tau)$ with the MSD $\langle r^2\rangle$ calculated in the diffusive regime ($t > 50\tau$).

The diffusion constant of a typical small solute such as an ion or a small molecule is $D \approx 1$ nm^2/ns, which is $D \approx 0.078\lambda^2/\tau$ in the standard DPD units ($\lambda = 0.646$ nm, $\tau = 0.029$ ns). Our simulation data confirm that by choosing the mass of the solute particles the same as the mass of the DPD particles, the dynamics are already fully in the diffusive regime at $\langle r^2\rangle = \lambda^2$ (Fig. 3). As expected, the dynamics do not depend on specific γ_s and r_s as long as D is kept constant. The transition from ballistic to diffusive dynamics occurs on the lengthscale $r_{BD} = 2\sqrt{3}D\tau/\lambda \approx 0.27\lambda$ (Fig. 3). Therefore, we conclude that the standard DPD friction $\gamma = 4.5k_BT\tau r_c^{-2}$ models the appropriate diffusive dynamics on the relevant lengthscales ($r \geq \lambda$).

If necessary, the ballistic–diffusive transition τ_{BD} can be pushed to even smaller values by increasing the DPD solvent friction γ or decreasing the solute mass, but both would require a smaller integration time-step, decreasing the efficiency. Conversely, if a larger ballistic regime is permitted, γ could be decreased, which would reduce the DPD viscosity and, thus, increase the value of the time unit τ, allowing exploration of longer timescales, but that would also reduce the Schmidt number (Sc), which may be important; see discussion below.

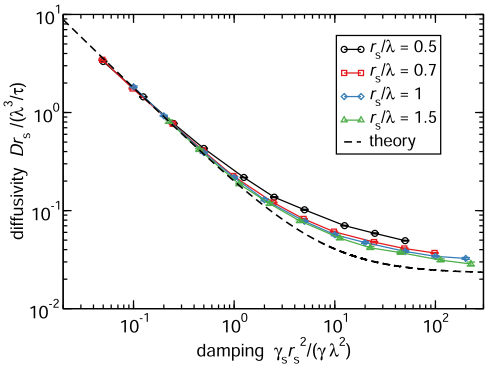

FIG. 2. Master plot of diffusivity data from simulations (symbols) and comparison to the analytical prediction [dashed line, Eq. (7)].

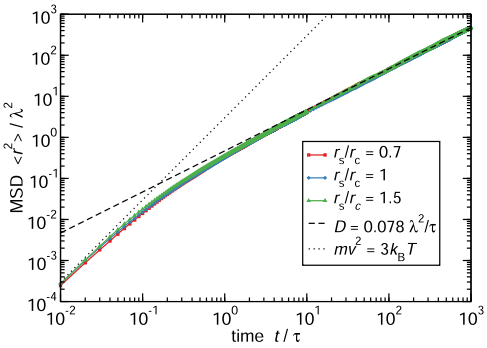

FIG. 3. Mean-squared displacement (MSD) of solutes in bulk solution for different r_s at $D \approx 0.078\lambda^2/\tau$. $[r_s, \gamma_s] = [0.7\lambda, 30\gamma]$ (red squares), $[\lambda, 5\gamma]$ (blue diamonds), and $[1.5\lambda, \gamma]$ (green triangles), showing the ballistic-to-diffusive transition does not explicitly depend on γ_s and r_s, but only on D.

A. Limitation of the method: Solute permeability

The main limitation of using only dissipative and random forces for the solute–solvent interaction is that solutes are not impermeable to the solvent particles. The coupling γ_s effectively determines the local viscosity at the location of the solute particle, but the solvent can pass through the solute. This is illustrated by the velocity profiles around a spherical solute (Fig. 4). Larger coupling γ_s leads to smaller fluid velocity at the particle location. In the limit $\gamma_s \to \infty$, the solute becomes effectively impermeable. In this sense, DPDS bears similarities to the MPC[2] and FPD[4] methods.

The effect of permeability can be systematically investigated by choosing different r_s, γ_s that yield the desired diffusion constant (Fig. 4). At large γ_s, the flow profile approaches the Oseen prediction for an impermeable spherical particle,[27]

$$v_x^b = v_0\left(1 + \frac{a^3}{2x^3} - \frac{3a}{2x}\right),$$
$$v_x^f = v_0\left(1 + \frac{a^3}{2x^3} - \frac{3a^2}{2x^2\,\mathrm{Re}}\left[1 - e^{-x\mathrm{Re}/a}\right]\right), \tag{8}$$

where v_x^b and v_x^f are the flow velocities behind and in front of the particle on the symmetry axis at $z = y = 0$. $v_0 = Df_{particle}/[k_BT(1 + 3\,\mathrm{Re}/8)]$ is the far field velocity at total force $f_{particle} = G_xL^3$, with G_x the body force on the fluid and L the system size (to calculate the flow profiles, the particle is immobilized and the force is applied to the fluid). The radius of a sphere that yields the desired diffusion constant D is $a = k_BT/(6\pi\eta D)$, and the corresponding Reynolds number is $\mathrm{Re} = a\rho v_0/\eta$. The simulated flow profiles approach the Oseen prediction for large γ_s [Fig. 4(d)]. The ratio $\gamma_s/\gamma = 5$ appears to be sufficiently large to reproduce the Oseen profile to a distance $r \approx 3/4\lambda$ and also the hydrodynamic scaling of polymer collapse, as shown below.

Another limitation of solute permeability concerns fast, time-dependent changes to the flow. The timescale of the solute–solvent coupling was calculated above, $\tau_{BD} = 2D\tau^2/\lambda^2$ and, thus, any temporal momentum change on timescales $t \leq \tau_{BD}$ will not be adequately transferred between solute and solvent. However, for standard DPD parameters and typical solute diffusivities, we find

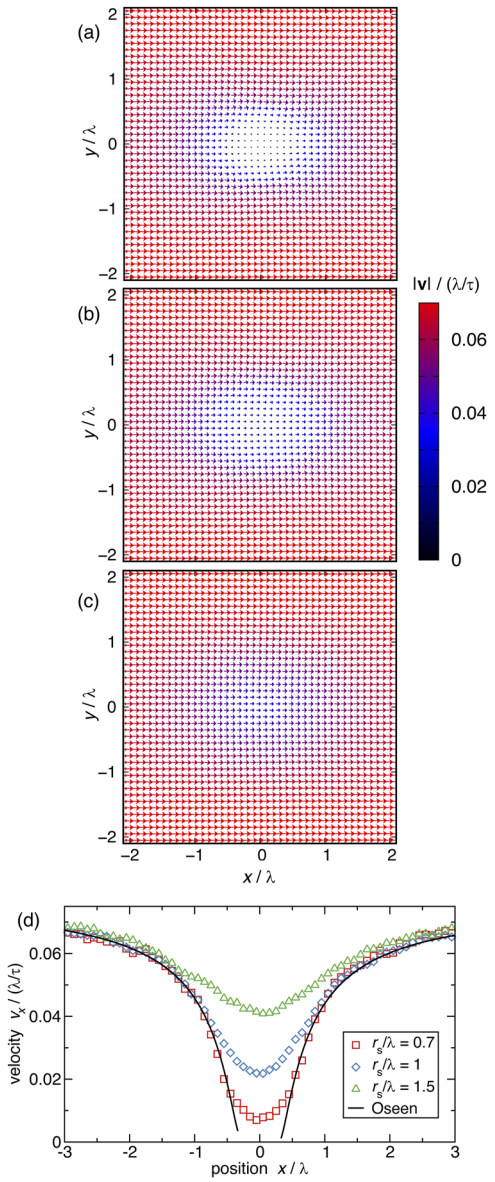

FIG. 4. Velocity profile around a spherical solute located at $x = y = z = 0$. (a)–(c) The three profiles are obtained at $[r_s, \gamma_s] = [0.7\lambda, 30\gamma]$ (a), $[\lambda, 5\gamma]$ (b), and $[1.5\lambda, \gamma]$ (c), corresponding to $D = 0.078\lambda^2/\tau$ (Fig. 3). The profiles are calculated by averaging the velocity of all DPD particles within $-0.1 < z/\lambda < 0.1$ for $t = 10^7\tau$. System size $L = 10\lambda$ with periodic boundary conditions and body force density $G_x = 10^{-3}k_BT/\lambda^4$ imposed on DPD particles. (d) The velocity v_x on the center line is obtained by averaging within $-0.1 < y/\lambda < 0.1$ and $-0.1 < z/\lambda < 0.1$. The Oseen analytical prediction (black line) is given by Eq. (8).

$\tau_{BD} < \tau$ (Fig. 3); the timescale of solute–solvent coupling is smaller than that of solvent–solvent coupling. Therefore, DPDS is not expected to introduce additional high-frequency limitations, and the standard DPDS parameters used here are sufficient for any perturbations slower than $\tau_{BD} \approx 10$ ps, which should be adequate for most applications. If even faster response times are required, τ can be reduced by increasing the thermostat friction γ.

If permeability is not allowed, for example, to model impermeable membranes, the repulsive interactions between solute and solvent can be added to the model. This is partially achieved by the standard DPD approach, where solute–solvent interaction, e.g., for membrane lipids[13] or polymers,[14] is also represented as soft repulsion [Eq. (1)]. Full blocking could be achieved by hard repulsive interaction such as Lennard-Jones or Weeks-Chandler-Andersen (WCA). In either case, the solute–solvent conservative interactions change the equilibrium distributions of the solutes and induce entropic depletion interactions between solutes if solutes and solvent particles are not of the same size. This likely requires that the solute model be designed and parameterized for specific DPD solvent parameters.

B. Recipe

We provide a straightforward recipe on how to use the DPDS method with coarse-grained models of solutes.

1. Choose the desired solvent properties: determine the minimum DPD length scale r_c on which to resolve hydrodynamics and obtain the desired compressibility via a_{ij}.[9] Choose the thermostat coupling γ that results in the desired transition between ballistic and diffusive regimes. The standard parameters $r_c = 0.646$ nm, $\rho = 3r_c^{-3}$, $a_{ij} = 78k_BT$, and $\gamma = 4.5\sqrt{k_BTm}/r_c$ are likely a good starting point for most coarse-grained models of aqueous solutions of molecules, ions, and polymers.
2. Determine the solute–solvent coupling, r_s and γ_s, that yields the desired solute diffusivity D: The size r_s should be similar to the physical size of the solutes, and γ_s is determined via Eq. (7) or by measuring the mean-squared displacement of solutes.

This introduces both hydrodynamic interactions and thermostating of the solute system while maintaining the equilibrium configurational distribution of the solutes. An example implementation in the open-source MD package LAMMPS is provided in the Appendix.

IV. APPLICATIONS

To demonstrate the applicability of the DPDS method, we investigate two different systems where hydrodynamic interactions play a crucial role: the collapse and diffusion dynamics of a single polymer and the electroosmotic flow of an electrolyte solution.

A. Polymer dynamics

We consider a bead–spring polymer model[24] in an aqueous solution. Consecutive beads in a polymer chain of N beads are connected via a harmonic potential,

$$U = \frac{K}{2}(r_{ij} - \lambda)^2, \tag{9}$$

with zero-energy bond length λ and strength $K = 100k_BT/\lambda^2$.

The polymer is immersed in a DPD solvent described by the standard parameters for an aqueous solution ($\rho = 3r_c^{-3}$, $\gamma = 4.5k_BT\tau/r_c^2$, $a_{ij} = 78k_BT$, and $r_c = \lambda = 0.646$ nm). The coupling

between the polymer beads and the DPD fluid is achieved with $\gamma_s = 5\gamma$ and $r_s = r_c$, which models the diffusion constant of individual monomers $D = 1.1$ nm^2/ns (Fig. 1). The system is evolved using the velocity-Verlet integrator with a time step of $\Delta t = 0.005\tau$.

First, we measure the diffusion constant for different polymer sizes and compare the scaling with the Zimm dynamics prediction $D \propto N^{-\nu}$, with ν the scaling exponent; $\nu = 0.588$ at good-solvent conditions.[28] The system is a cubic box with a size of $L = 100\lambda$ and periodic boundary conditions. Polymers of length N and monomer density $\rho_m = 10^{-3}/\lambda^3$ are equilibrated under good solvent conditions. Bead–bead repulsion is modeled as a Lennard-Jones (WCA) interaction with size $\sigma = \lambda$, strength $\varepsilon = k_BT$, and cutoff $r_{cut} = 2^{1/6}\sigma$. We measure the mean-squared-displacement of all monomers $\langle r^2 \rangle$ for $t = 5000\tau$. The diffusion constant is measured via the slope of the average mean squared-displacement as a function of time, $6D = \partial\langle r^2\rangle/\partial t$; at large displacements, $\langle r^2\rangle > (2R_g)^2$.

The scaling of the diffusion constant with size fully reproduces the expected Zimm dynamics (Fig. 5). Small deviations (<10%) occur for very short polymers ($N \sim 1$) due to finite size effects.

We next measure the timescale of a hydrophobic collapse of the polymer, a problem related to the dynamics of protein folding. Analytical predictions for the hydrophobic collapse timescale τ_c of an initially expanded polymer indicate $\tau_c \sim N^2$ for Brownian dynamics and $\tau_c \sim N^{4/3}$ with hydrodynamics[29] since a polymer globule needs to travel a distance $\sim N$ while the drag on the collapsed globules scales as $\sim N$ for Brownian dynamics and $\sim N^{1/3}$ for Stokes flow.

The collapse timescale τ_c is defined by the time required for the change in the radius of gyration $R_g(t)$ to reach a fraction $f_c = 0.9$ of the maximum change,

$$R_g(\tau_c) = (1 - f_c)R_{g,0} + f_c R_{g,col}, \tag{10}$$

where $R_{g,0}$ and $R_{g,col}$ are, respectively, the initial and the final (collapsed) R_g values. We consider two initial configurations: (i) a fully expanded linear polymer ($R_{g,0} \sim N$) and (ii) a polymer equilibrated at good solvent conditions ($R_{g,0} \sim N^{\nu}$) with the scaling exponent $\nu = 0.588$. To model the collapse, we introduce attractive interactions between monomers modeled by the Lennard-Jones potential with size $\sigma = \lambda$, strength $\varepsilon = 1.25k_BT$, and cutoff $r_{LJcut} = 2.5\sigma$, which introduces a sudden quench in solvent quality. We can estimate the Flory–Huggins χ parameter by matching the critical point of the Lennard-Jones fluid, $T_{c,LJ} \approx 1.3\varepsilon/k_B$, to the regular solution model, yielding $\chi \approx 2T_{c,LJ}/T$. For $\varepsilon = 1.25k_BT$, this results in $\chi \approx 3.25$, which is sufficiently large to drive polymer collapse.

Simulation data shown in Fig. 6 show the scaling follows $\tau_c \sim N^{1.42\pm0.02}$ for an initially fully stretched polymer, while $\tau_c \sim N^{0.95\pm0.05}$ for an initially equilibrated polymer. The first scaling exponent is close to the analytical prediction for an expanded polymer $N^{4/3}$, and the second agrees with previous DPD predictions for an equilibrated polymer,[14] $\tau_c \sim N^{0.98\pm0.09}$.

To further validate the DPDS method, we compare it with the standard DPD approach. We perform collapse simulations of a neutral polymer using the standard DPD model, where the conservative monomer–monomer and monomer–solute interactions are described by the DPD potentials [Eq. (1)] and thermostat with $\gamma = 4.5k_BT\tau r_c^{-2}$ is applied between all pairs of particles. The interaction strength is described by the prefactor a_{ij}, where i denotes a solute and j is a solvent. We use $a_{jj} = a_{ij} = 78k_BT$. The polymer is equilibrated in good solvent conditions ($a_{ii} = 85k_BT$), and the collapse is then initiated by changing the monomer–monomer interaction to $a_{ii} = 65k_BT$, thereby reducing the solvent quality. The interaction difference $a_{ij} - a_{ii} = 13k_BT$ results in the χ parameter[9] of $\chi \approx 3.5$, which is very close to the above estimate for the

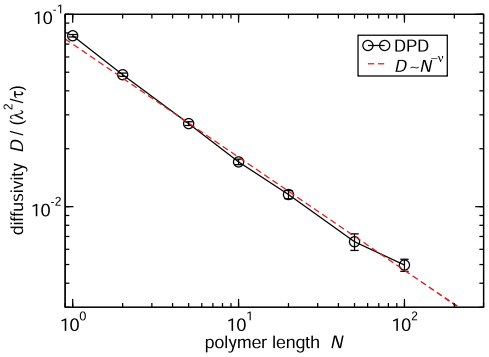

FIG. 5. Diffusion constant D depends on polymer size N. Simulation data (black circles) is well described by Zimm dynamics (red dashed line) with the good-solvent scaling exponent $\nu = 0.588$. Error bars denote standard errors obtained from eight independent simulations.

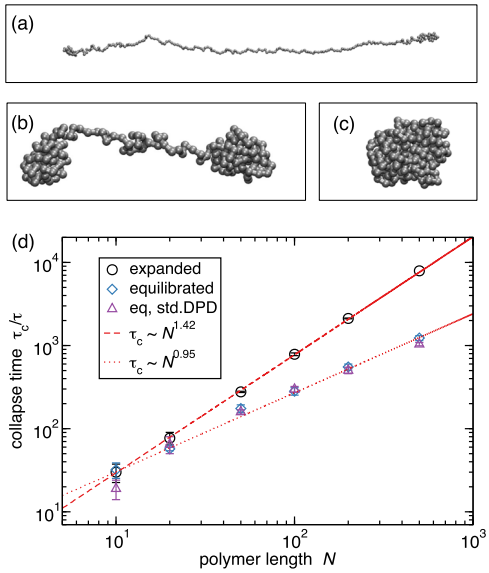

FIG. 6. Polymer collapse. (a)–(c) configurations of a bead–spring polymer of size $N = 200$ during collapse from an initially fully expanded linear chain at (a) $t = 500\tau$, (b) $t = 2000\tau$, and (c) $t = 2500\tau$. (d) DPDS simulation data showing collapse timescale dependence on the polymer size N for an initially expanded linear chain (black circles), which follows $\sim N^{1.42\pm0.02}$ scaling, and an initially equilibrated polymer at good solvent conditions (blue diamonds), which follows $\sim N^{0.95\pm0.05}$. For comparison, we show the collapse data using the standard DPD model with soft-repulsive beads (purple triangles). System size for the initially expanded case is $L_x = N + 10\lambda$, $L_y = L_z = 50\lambda$, and for equilibrated polymers, $L_x = L_y = L_z = 80\lambda$. Error bars denote standard errors obtained from five (black circles) and 20 (blue diamonds and purple triangles) independent simulations.

Lennard-Jones model. The collapse timescales using the standard DPD approach agree with the DPDS method and Lennard-Jones polymer model (Fig. 6).

This data on polymer diffusion and collapse timescales indicates that the DPDS method faithfully reproduces the hydrodynamic coupling between a polymer and a solvent. Contrary to standard DPD, the DPDS method combined with the Lennard-Jones interaction (or a similar hard repulsive interaction) allows straightforward addition of point charges and simulation of polyelectrolytes.[30]

B. Nanochannel flow

We next consider the electro-osmotic flow of an electrolyte solution in a slit nanochannel and investigate the coupling between hydrodynamics and electrostatic interactions. To use DPDS for wall-bounded flows, we must first briefly discuss a method to impose a desired no-slip or slip boundary condition at the channel walls.

1. Wall boundary condition

To impose the desired boundary condition on the channel walls, we investigate a pure solvent system without ions. Implementation of solid walls within DPD simulations is not straightforward due to layering artifacts that can occur next to a flat wall.[31] A no-slip boundary condition can be imposed by introducing a layer of immobilized DPD particles at the walls;[32] however, due to repulsive interactions, the slip length dependence on the wall particle density is non-monotonic. Another possibility is to impose a drag force parallel to the wall.[33,34]

Here, we propose an alternative strategy to impose a boundary condition by coupling the DPD fluid to the immobilized wall particles only through the thermostat with coupling strength γ_w, which is determined by the desired slip-length. The method is very similar to using a parallel drag force[33] but is expected to be easier to employ because it does not require separate implantation of a wall–DPD thermostat.

The DPD solvent particles interact with a smooth repulsive surface via a repulsive WCA interaction with $\sigma = r_c$ and $\varepsilon = k_B T$. The smooth repulsive surfaces are positioned at $y_{wall} = \pm(w/2 + r_c)$, where w is the width of the nanochannel. In addition, immobile particles are placed at the wall surface $y_{im} = \pm w/2$, at 2D density $\rho_w = \rho r_c$, arranged on a regular mesh with lattice spacing $a_w = \rho_w^{-1/2}$. These immobile particles interact with the DPD particles only via the DPD thermostat with strength γ_w and range r_c [Eqs. (2), (3), and (5)].

To induce flow, a pressure gradient G_x is imposed on the fluid as a body force, $f_x = G_x/\rho$, which acts on each DPD particle. The system size is $L_y = L_z = \mathrm{w}$ and $L_x = 40\lambda$, with periodic boundary conditions in x and z. The system is simulated for $t_{init} = 5000\tau$ to reach a steady state, followed by $t = 5 \cdot 10^5 \tau$ for calculation of the velocity profiles at different values of the wall–solvent coupling γ_w (Fig. 7).

The velocity profile between two parallel plates at low Reynolds numbers follows the parabolic Poiseuile profile,

$$v(y) = \frac{G_x}{2\eta}(w^2/4 - y^2 + wL_s). \tag{11}$$

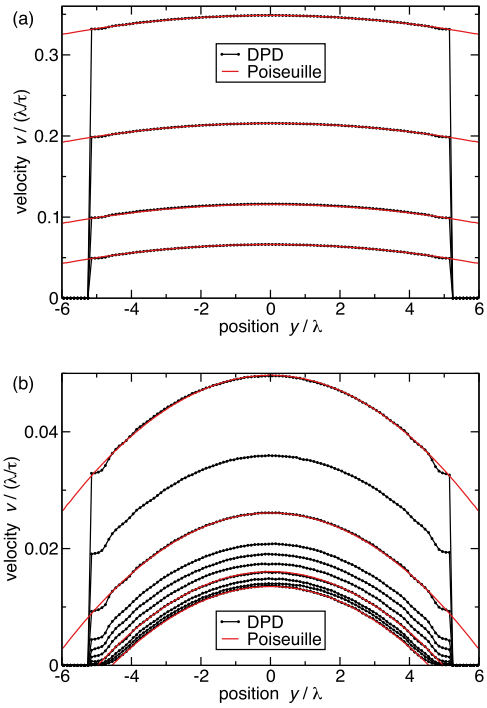

FIG. 7. Velocity flow profile from DPD simulations (black circles) and comparison to Poiseuille profiles (red curves) given by Eq. (11). (a) and (b) DPD data (black) from bottom to top are obtained at $\gamma_w/\gamma = [5, 3, 2, 1, 0.5, 0.3, 0.2, 0.1, 0.05, 0.03, 0.02, 0.01, 0.005, 0.003]$ at pressure gradient $G_x = 0.003 k_B T/\lambda$ and $w = 10\lambda$. Poiseuille prediction (red curves) from bottom to top shown for slip length $L_s/\lambda = [-0.42, -0.03, 1.52, 5.15, 7.7, 15.3, 30.7, 51.2]$ at viscosity $\eta = 2.31 k_B T\tau/\lambda^3$ [Eq. (13)].

The slip length,

$$L_s = \pm\Delta v \left[\left(\frac{\partial v}{\partial y}\right)_{y=\mp w/2}\right]^{-1}, \tag{12}$$

is determined by the slip velocity Δv at the wall. We find the simulated velocity profiles accurately reproduce the parabolic Poiseuille profiles for at least two orders of magnitude in flow velocity and slip lengths from zero to larger than channel width (Fig. 7). A small deviation from the parabolic profile is observed within a distance r_c of the wall due to the layering effect of the DPD particles next to a smooth, repulsive wall.

To avoid numerical errors when calculating derivatives [Eq. (12)], we determine the slip length from averages in the velocity. Since the velocity profiles are parabolic (Fig. 7), the slip length can be obtained by integrating the profile [Eq. (11)],

$$L_s = \left(\frac{\bar{v}}{\bar{v}_P} - 1\right)\frac{w}{6}, \tag{13}$$

where $\bar{v}$ is the average velocity in the channel and

$$\bar{v}_P = \frac{G_x w^2}{12\eta} \tag{14}$$

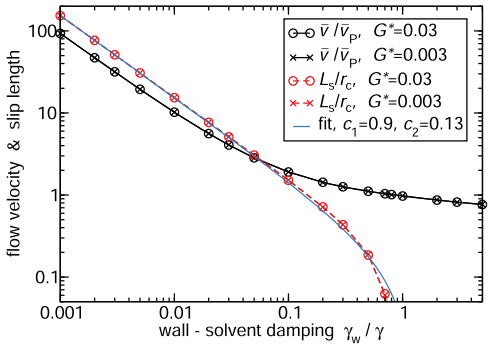

FIG. 8. Average velocity obtained from simulations (solid black line) and corresponding slip length using Eq. (13) (dashed red lines) using viscosity $\eta = 2.31 k_B T \tau / \lambda^3$. The data for different pressure gradients $G^* = G_x / k_B T \rho \lambda$ show perfect overlap. The two parameter fit [Eq. (15)] (solid blue line) is accurate to within $0.1 r_c$.

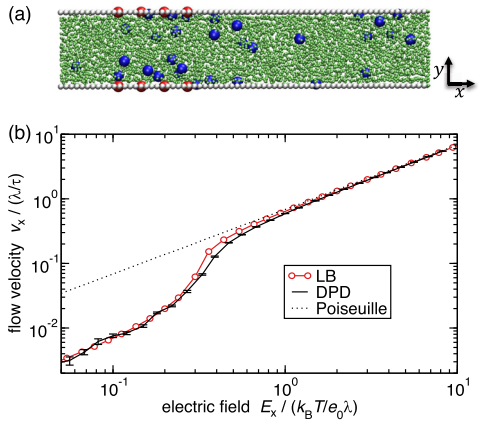

FIG. 9. Electroosmotic flow in a slit channel. (a) Configuration setup showing DPD particles (green), immobile wall particles (white), surface charge (red), and counterions (blue). (b) Mean velocity in a slit channel obtained from DPD simulations and comparison to lattice-Boltzmann (LB) and Poiseuille prediction [Eq. (14)] at driving force $G_x = E_x e_0 \rho_{ion}$. Slip length $L_s \approx 30\lambda$ is obtained at $\gamma_w = 0.005\gamma$ in DPD, and fractional bounce-back $f_{bb} = 0.99$ in LB.

is the average velocity for the Poiseuille profile at $L_s = 0$. Thus, we obtain the slip length as a function of wall damping γ_w (Fig. 8).

Analytical considerations show that in the second order, the slip length is given by

$$L_s / r_c = c_1 / \alpha - c_2 - \mathcal{O}(\alpha), \tag{15}$$

with $\alpha = r_c^2 \gamma_w \rho / \eta$[33] and the positive constants c_1, c_2 of order unity that depend on the wall solvent interaction. We find that fitting $c_1 = 0.9$ and $c_2 = 0.13$ can be used to predict L_s with accuracy within $0.1 r_c$ (Fig. 8).

2. Electroosmotic flow

Having described the channel setup and the wall interaction, we show how to simulate the hydrodynamic flow of an electrolyte. Free monovalent ions are modeled as charged spheres with short-range ion–ion repulsion modeled by the WCA potential with hydrated ion diameter $\sigma = \lambda = 0.646$ nm and interaction strength $\varepsilon = k_B T$. The experimentally measured value for small-ion diffusivity, $D \approx \text{nm}^2/\text{ns}$, is obtained at solvent–solute coupling strength $\gamma_s = 5\gamma$ and range $r_s = \lambda$ (Fig. 3). The electrostatic interactions are calculated using particle-particle particle-mesh (PPPM) Ewald summation with a real-space cutoff $r_{ewald} = 5\lambda$ and a relative force accuracy of 10^{-4}. Slab correction factor 3.0 is used in the y coordinate to simulate fixed boundary conditions at the channel walls. Electrostatic strength is determined by the Bjerrum length $l_B = 0.71$ nm, which corresponds to an aqueous solution at room temperature.

We consider an electroosmotic flow in a nanochannel of width $w = 8\lambda$ under an external electric field E_x. To investigate a nonsymmetric case where the accurate description of convection and diffusion of ions is important, the wall contains a small charged section that covers a fraction $f_w = 0.25$ of the wall surface with charge density, $\sigma_q = 0.2 e_0 / \lambda^2$ [see Fig. 9(a)]. The solution contains counter-ions at density $\rho_{ion} = 2\sigma_q f_w / w$. This configuration introduces a pattern in the charge density and Poisson–Boltzmann (PB) calculations predict two distinct regimes due to the localization of counter-ions at small external fields.[35] This effect is pronounced at non-zero slip lengths, and we use $L_s = 30\lambda$, a typical order of magnitude for the slip length of an aqueous solution.[36]

The DPDS results are in excellent agreement with PB simulations and clearly show two distinct flow regimes (Fig. 9). The PB calculations are performed by employing the *Ludwig* open-source package with electrokinetics[37] using lattice size $\Delta x = \lambda/2$, reduced viscosity $\eta^* = 0.2$, and parameters corresponding to the kinematic viscosity of water $\nu_k = 10^{-6}\ \text{m}^2/\text{s}$. The desired slip length is obtained via a fractional bounce-back boundary condition[38] with fraction f_{bb}. All other parameters are the same as described for DPD. Small deviations between DPD and PB occur at the transition between the two flow regimes, which we attribute to the lack of thermal fluctuations in the PB model as well as the lattice approximation and the associated lack of unit charge discretization in PB. However, the flow velocity in the two regimes is in perfect agreement.

These results demonstrate the applicability of DPDS to model the hydrodynamics of electrolyte solutions. When considering a highly concentrated solution, the viscosity typically increases with electrolyte concentration. This effect is captured by the DPDS method, and the rate of viscosity increases with concentration depending on the solute–solvent thermostat coupling length r_s [Eq. (6)]. Thus, the value of r_s could be chosen to obtain the desired quantitative relation between viscosity and solute concentration. Moreover, direct thermostat coupling [Eqs. (2) and (3)] between solutes could be added to further increase the viscosity of highly concentrated solutions.

V. SUMMARY

In summary, we proposed a DPD-solvent (DPDS) method that introduces solvent hydrodynamics to coarse-grained models of solutes. The solute–solvent interaction occurs only via dissipative and random forces, which ensures the equilibrium configurational properties of the solute system are not affected by the presence of the DPD solvent. The solute–solvent coupling strength is determined by the desired diffusion constants of the solute. Because the method

is based on short-ranged DPD interactions, the computational cost scales linearly with the system size.[39]

The DPDS method can be utilized as a replacement for a Nosé–Hoover or Langevin thermostat in coarse-grained MD simulations while capturing the hydrodynamic interactions at the desired solvent compressibility, viscosity, and solute diffusivity (see Sec. III B). The examples shown demonstrate that the method reproduces the correct hydrodynamics of Oseen flow, channel flow, electroosmotic effects, and polymer hydrodynamics. Moreover, since the method utilizes the standard DPD thermostat, the simulations can be performed using existing implementations in open-source molecular dynamics packages such as LAMMPS and ESPResSo. Thus, the method should be broadly useful as a means to introduce hydrodynamics to existing coarse-grained models of molecules and soft materials.

The method could be used with multicomponent solvents that are described by two or more different types of DPD particles.[12,40] In this case, the solute–solvent coupling could be distinct among different solvents, modeling different diffusivities. In addition, the chemical potential differences of the solutes in different solvents could be introduced by soft solute–solvent interactions. While we have only considered solute models based on spherical excluded-volume interactions, such as ions or monomers in polymers, the method can be applied to non-spherically symmetric solutes, for example, by uniformly distributing ghost particles inside a non-spherical object and coupling these ghost particles to the DPD solvent via Eqs. (2) and (3).

ACKNOWLEDGMENTS

I thank Ignacio Pagonabarraga, James D. Farrell, and Jiaxing Yuan for their discussions and comments on the manuscript. This work was supported by the startup funds provided by the Whiting School of Engineering at JHU and performed using the Advanced Research Computing at Hopkins (rockfish.jhu.edu), which is supported by the National Science Foundation (NSF) Grant No. OAC 1920103.

AUTHOR DECLARATIONS

Conflict of Interest

The author has no conflicts to disclose.

Author Contributions

Tine Curk: Writing – original draft (lead).

DATA AVAILABILITY

The data that support the findings of this study are available within the article.

APPENDIX: DPDS IMPLEMENTATION IN LAMMPS

Implementation of the DPDS in the LAMMPS open-source MD package can be achieved using the existing `dpd` or `dpd/ext` pair styles.[41] Let us assume that type 1 is the solvent and type 2 is the solute, and hybrid/overlay is used to combine DPD interactions with the solute–solute interactions. For the solute–solvent, polymer–solvent, and ion–solvent interaction cases discussed in Secs. II and III [using the Lennard-Jones (LJ) reduced units with unit length $\lambda = r_c = 1$ and DPD particle density $\rho = 3\lambda^{-3}$], the solvent properties are determined by the DPD model:

`pair_coeff 1 1 dpd/ext` $a_{ij}\gamma\ \gamma_\perp$ `1 1 1.0`

while the solute–solvent coupling is determined by the thermostat:

`pair_coeff 1 2 dpd/ext/tstat` $\gamma_s\gamma_{\perp,s}$ `1 1` r_s/λ

Combining these instructions with the desired solute–solute interactions and a velocity-Verlet integrator introduces hydrodynamic interactions without affecting the equilibrium canonical distribution of the solute particles, as compared to using a Langevin or Nosé–Hoover thermostat.

REFERENCES

[1] A. Malevanets and R. Kapral, "Mesoscopic model for solvent dynamics," J. Chem. Phys. **110**, 8605–8613 (1999).
[2] G. Gompper, T. Ihle, D. M. Kroll, and R. G. Winkler, "Multi-particle collision dynamics: A particle-based mesoscale simulation approach to the hydrodynamics of complex fluids," in *Advanced Computer Simulation Approaches for Soft Matter Sciences III*, edited by C. Holm and K. Kremer (Springer, Berlin, Heidelberg, 2009), pp. 1–87.
[3] T. Krueger, H. Kusumaatmaja, A. Kuzmin, O. Shardt, G. Silva, and E. M. Viggen, *The Lattice Boltzmann Method: Principles and Practice*, *Graduate Texts in Physics* (Springer, 2016).
[4] H. Tanaka and T. Araki, "Simulation method of colloidal suspensions with hydrodynamic interactions: Fluid particle dynamics," Phys. Rev. Lett. **85**, 1338–1341 (2000).
[5] B. Dünweg and A. J. C. Ladd, "Lattice Boltzmann simulations of soft matter systems," in *Advanced Computer Simulation Approaches for Soft Matter Sciences III*, edited by C. Holm and K. Kremer (Springer, Berlin, Heidelberg, 2009), pp. 89–166.
[6] A. Furukawa, M. Tateno, and H. Tanaka, "Physical foundation of the fluid particle dynamics method for colloid dynamics simulation," Soft Matter **14**, 3738–3747 (2018).
[7] T. Soddemann, B. Dünweg, and K. Kremer, "Dissipative particle dynamics: A useful thermostat for equilibrium and nonequilibrium molecular dynamics simulations," Phys. Rev. E **68**, 046702 (2003).
[8] P. J. Hoogerbrugge and J. M. V. A. Koelman, "Simulating microscopic hydrodynamic phenomena with dissipative particle dynamics," Europhys. Lett. **19**, 155 (1992).
[9] R. D. Groot and P. B. Warren, "Dissipative particle dynamics: Bridging the gap between atomistic and mesoscopic simulation," J. Chem. Phys. **107**, 4423–4435 (1997).
[10] P. Espanol and P. B. Warren, "Perspective: Dissipative particle dynamics," J. Chem. Phys. **146**, 150901 (2017).
[11] R. D. Groot, "Electrostatic interactions in dissipative particle dynamics—Simulation of polyelectrolytes and anionic surfactants," J. Chem. Phys. **118**, 11265–11277 (2003).
[12] I. Pagonabarraga and D. Frenkel, "Dissipative particle dynamics for interacting systems," J. Chem. Phys. **115**, 5015–5026 (2001).
[13] R. Groot and K. Rabone, "Mesoscopic simulation of cell membrane damage, morphology change and rupture by nonionic surfactants," Biophys. J. **81**, 725–736 (2001).
[14] J. Guo, H. Liang, and Z.-G. Wang, "Coil-to-globule transition by dissipative particle dynamics simulation," J. Chem. Phys. **134**, 244904 (2011).

[15]C. Junghans, M. Praprotnik, and K. Kremer, "Transport properties controlled by a thermostat: An extended dissipative particle dynamics thermostat," Soft Matter **4**, 156–161 (2008).
[16]I. Pagonabarraga, M. H. J. Hagen, and D. Frenkel, "Self-consistent dissipative particle dynamics algorithm," Europhys. Lett. **42**, 377 (1998).
[17]K. P. Santo and A. V. Neimark, "Dissipative particle dynamics simulations in colloid and interface science: A review," Adv. Colloid Interface Sci. **298**, 102545 (2021).
[18]N. Lauriello, J. Kondracki, A. Buffo, G. Boccardo, M. Bouaifi, M. Lisal, and D. Marchisio, "Simulation of high Schmidt number fluids with dissipative particle dynamics: Parameter identification and robust viscosity evaluation," Phys. Fluids **33**, 073106 (2021).
[19]N. A. Spenley, "Scaling laws for polymers in dissipative particle dynamics," Europhys. Lett. **49**, 534 (2000).
[20]R. C. Krafnick and A. E. Garcia, "Efficient Schmidt number scaling in dissipative particle dynamics," J. Chem. Phys. **143**, 243106 (2015).
[21]C. P. Lowe, "An alternative approach to dissipative particle dynamics," Europhys. Lett. **47**, 145–151 (1999).
[22]A. Boromand, S. Jamali, and J. M. Maia, "Viscosity measurement techniques in dissipative particle dynamics," Comput. Phys. Commun. **196**, 149–160 (2015).
[23]Using this timescale we can determine the mass of the particles and find $m \approx 8.310^{-24}$ kg, which is about two orders of magnitude larger than the mass of three water molecules. This is a consequence of the low Schmidt number at the standard DPD parameters and the requirement to model the desired dynamic viscosity η.
[24]M. J. Stevens and K. Kremer, "The nature of flexible linear polyelectrolytes in salt free solution: A molecular dynamics study," J. Chem. Phys. **103**, 1669–1690 (1995).
[25]S. J. Marrink, H. J. Risselada, S. Yefimov, D. P. Tieleman, and A. H. de Vries, "The MARTINI force field: Coarse grained model for biomolecular simulations," J. Phys. Chem. B **111**, 7812–7824 (2007).
[26]B. E. K. Snodin, F. Randisi, M. Mosayebi, P. Šulc, J. S. Schreck, F. Romano, T. E. Ouldridge, R. Tsukanov, E. Nir, A. A. Louis, and J. P. K. Doye, "Introducing improved structural properties and salt dependence into a coarse-grained model of DNA," J. Chem. Phys. **142**, 234901 (2015).
[27]G. K. Batchelor, *An Introduction to Fluid Dynamics* (Cambridge University Press, Berlin, Heidelberg, 1967).
[28]M. Rubinstein and R. H. Colby, *Polymer Physics* (Oxford University Press, New York, 2003), Vol. 23.
[29]N. Kikuchi, J. F. Ryder, C. M. Pooley, and J. M. Yeomans, "Kinetics of the polymer collapse transition: The role of hydrodynamics," Phys. Rev. E **71**, 061804 (2005).
[30]J. Yuan and T. Curk, "Collapse and expansion kinetics of a single polyelectrolyte chain with hydrodynamic interactions," J. Chem. Phys. **160**, 161103 (2024).
[31]I. V. Pivkin and G. E. Karniadakis, "A new method to impose no-slip boundary conditions in dissipative particle dynamics," J. Comput. Phys. **207**, 114–128 (2005).
[32]E. I. Barcelos, S. Khani, A. Boromand, L. F. Vieira, J. A. Lee, J. Peet, M. F. Naccache, and J. Maia, "Controlling particle penetration and depletion at the wall using dissipative particle dynamics," Comput. Phys. Commun. **258**, 107618 (2021).
[33]J. Smiatek, M. P. Allen, and F. Schmid, "Tunable-slip boundaries for coarse-grained simulations of fluid flow," Eur. Phys. J. E **26**, 115–122 (2008).
[34]J. Smiatek, M. Sega, C. Holm, U. D. Schiller, and F. Schmid, "Mesoscopic simulations of the counterion-induced electro-osmotic flow: A comparative study," J. Chem. Phys. **130**, 244702 (2009).
[35]T. Curk, S. G. Leyla, and I. Paganobarraga, "Discontinuous transition in electrolyte flow through charge-patterned nanochannels," arXiv:2401.03666 (2024).
[36]P. Joseph and P. Tabeling, "Direct measurement of the apparent slip length," Phys. Rev. E **71**, 035303 (2005).
[37]F. Capuani, I. Pagonabarraga, and D. Frenkel, "Discrete solution of the electrokinetic equations," J. Chem. Phys. **121**, 973–986 (2004).
[38]K. Wolff, D. Marenduzzo, and M. E. Cates, "Cytoplasmic streaming in plant cells: The role of wall slip," J. R. Soc., Interface **9**, 1398–1408 (2012).
[39]D. Frenkel and B. Smit, *Understanding Molecular Simulation*, 2nd ed. (Academic, San Diego, 2002).
[40]S. Merabia, J. Bonet-Avalos, and I. Pagonabarraga, "Modelling capillary phenomena at a mesoscale: From simple to complex fluids," J. Non-Newtonian Fluid Mech. **154**, 13–21 (2008).
[41]A. P. Thompson, H. M. Aktulga, R. Berger, D. S. Bolintineanu, W. M. Brown, P. S. Crozier, P. J. in't Veld, A. Kohlmeyer, S. G. Moore, T. D. Nguyen, R. Shan, M. J. Stevens, J. Tranchida, C. Trott, and S. J. Plimpton, "LAMMPS—A flexible simulation tool for particle-based materials modeling at the atomic, meso, and continuum scales," Comput. Phys. Commun. **271**, 108171 (2022).